# Alkali-dissolving hydrothermal synthesis of zeolite P from fly ash

*Peng Wang*[1], *Qi Sun*[1] ✉, *Yujiao Zhang*[2], *Jun Cao*[1]

[1]*College of Materials and Metallurgy, Guizhou University, Guiyang 550025, People's Republic of China*
[2]*State Key Laboratory of Advanced Processing and Recycling of Non-ferrous Metals, Lanzhou University of Technology, Lanzhou, 730050, People's Republic of China*
✉ *E-mail: qsun@gzu.edu.cn*

Published in Micro & Nano Letters; Received on 24th October 2018; Revised on 16th January 2019; Accepted on 29th January 2019

Zeolite P with the pseudo-spherical form was successfully synthesised from low-grade fly ash via alkali-dissolving hydrothermal synthesis method. These samples were characterised by X-ray diffraction, scanning electron microscope, X-ray fluorescence, Fourier-transform infrared spectroscopy, thermogravimetry-differential scanning calorimeter (TG-DSC) and Brunauer–Emmett–Teller. The textural properties of zeolite P were further studied by $N_2$ adsorption–desorption technique. In addition, the TG-DSC study confirmed that the bound water content of zeolite P is 19.7% and the phase transition temperature of zeolite P is 400°C. Moreover, this thermal stability study approach not only extends the application of zeolite P but can be further extended to other zeolite materials as well.

**1. Introduction:** Fly ash (FA) is the by-product that comes from the inorganic components which inheres in coal and after high-temperature oxidates. Its main components are the aluminosilicate amorphous materials (proportion 60 to 80%), quartz and the after high temperatures formed mullite as well as a small amount of remnant unburned carbon material [1, 2]. Relevant data show that the cumulative stacking of FA in China has reached more than 600 million tons over the years. However, the total utilisation is <50% of the annual emission [3]. A large amount of remaining FA has been piled up or landfilled [4]. It is not only a waste of land resources but also results in a series of environmental problems [5–8]. In summary, using FA to produce high value-added products is a win–win development orientation between human beings and nature. We would obtain a series of new materials with better efficiency but lower prime cost. Holler and Wirsching [9] are the pioneers to synthesise zeolites from FA by hydrothermal method. Recently, Fukasawa *et al.* [10] proposed the syntheses of potassium-type zeolites from biomass incineration ash and coal FA via a hydrothermal route. Yi *et al.* [11] reported that zeolite P1 is synthesised from fluidised bed FA via a solvent-free process. Therefore, using FA to synthesise zeolite will be the focus in the near future.

Structure of zeolite P is composed of $[SiO_4]^{-4}$ and $[AlO_4]^{-5}$ tetrahedral units [12–19] which connected by an oxygen bridge. Take the shape through oxygen bridge to connect a kind of Gismondine type structure inorganic porous material which equipped with two-dimensional eight-membered ring cross-channel system. Furthermore, the apertures in the [100] and [010] directions are 0.31 nm × 0.44 nm and 0.26 nm × 0.49 nm, respectively [17, 20]. Compared with other porous materials, the surface of zeolite P was modified by the silicon hydroxyl group. The zeolite P with uniformly adjustable particle size is also equipped with a serious of eminent performance such as larger specific surface area, higher hydrothermal stability and uniform micropore. In summary, zeolite P has a wide range of applications in the fields of catalysts and adsorbents and so on [5, 17–19, 21–24].

Due to the framework structure of the alkaline zeolite, zeolite P has an excellent metal ion ($Ca^{2+}$, $Mg^{2+}$) exchange capacity and adsorption capacity [25]. Moreover, zeolite P is also equipped with higher non-ionic surfactant adsorption capacity which could improve the detergent formulations stability of certain expensive components. In conclusion, zeolite P is considered to be the most promising alternative about detergent builders [26].

In this Letter, zeolite P was synthesised from domestic FA by alkaline dissolution hydrothermal method. The starting material and the final product were analysed through X-ray diffraction (XRD), scanning electron microscope (SEM), thermogravimetry-differential scanning calorimeter (TG-DSC), X-ray fluorescence (XRF), Fourier-transform infrared spectroscopy (FTIR) and Brunauer–Emmett–Teller (BET). The physicochemical properties such as organisational appearance, chemical composition, specific surface area as well as thermal analysis were characterised in detail.

## 2. Materials and methods

2.1. Materials: The materials used in our research are as follows: solid sodium hydroxide (98%, AR), sodium aluminate ($Al_2O_3$ 45 wt. %, AR) and deionised water. The FA was provided by a Thermal Power Plant in China. The FA was passed through an 80 mesh sieve for the synthesis of zeolite.

2.2. Characterisation techniques: The major chemical compositions of the starting material and the final product were analysed using XRF(PANalytical B. V., AXIOSmAX). The element content was identified and quantified using inductively coupled plasma (ICP) atomic emission spectrometer (ICP, DSG-III). The phase and crystallinity of the sample were analysed by German Broker AXS D8-Focus, the instrument was Cu target, $\lambda$Cu K$\alpha$ = 0.15418 nm, tube voltage/current 30 kV/30 mA, monochromator Ni, scanning step size 0.02°, integration time 0.2 s. Infrared spectra of the starting material and the final product were analysed on a Nicolet iS50 FTIR spectrometer (Thermo Fisher America). The morphology of the starting material and the final product were analysed using an ultra-high resolution field emission SEM. The instrument used is SU8010 SEM, resolution: 1.3 nm, working distance: 0.5–30 mm, working voltage: 0.1–30 kV. The textural properties of the final product were measured using an ASAP2020 specific surface area analyser (Micromeritics, America). The thermal stability was recorded using an Netzsch STA 409 PC integrated thermal analyser.

2.3. Preparation of zeolite P: A certain amount of calcined FA was placed in a clean beaker. Also a certain amount of solid sodium hydroxide was weighed and dissolved to be the solution. The calcined FA and the sodium hydroxide solution were added into the 150 ml Erlenmeyer flask together before reacted in an oil bath. The mixture was placed to reaction at 90°C for 12 h with stirring constantly at 400 r $min^{-1}$. The mixture was filtered after




doi: 10.1049/mnl.2018.5650

completion of the reaction. The filtered residue was used to prepare zeolite P by hydrothermal reaction. The concentration of silica-alumina in the filtrate was chemically analysed using ICP. A certain concentration of sodium aluminate solution was prepared and added dropwise to the filtrate. After stirring at room temperature for 30 min, and the mixture was transferred to an autoclave for reaction. Afterward, the mixture was filtered, washed and dried to obtain zeolite P. Fig. 1 shows the flow diagram of the synthesis of zeolite P.

## 3. Results and discussion

3.1. Structural and chemical composition analysis: Fig. 2 presents the XRD patterns of FA and calcined FA as well as synthetic zeolite P. From the $2\theta$ values of the diffraction peaks in FA and calcined FA, it is known that the main crystalline components of FA

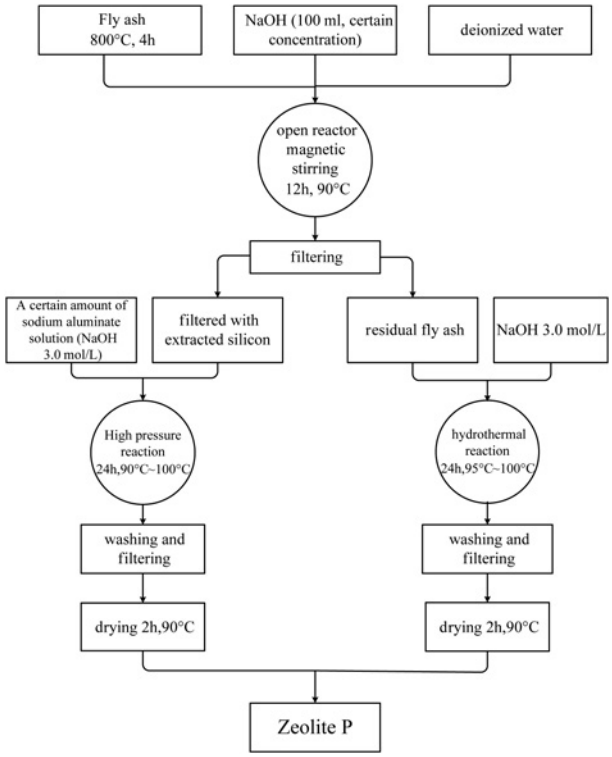


**Fig. 1** *Flow diagram of the zeolite synthesis P*

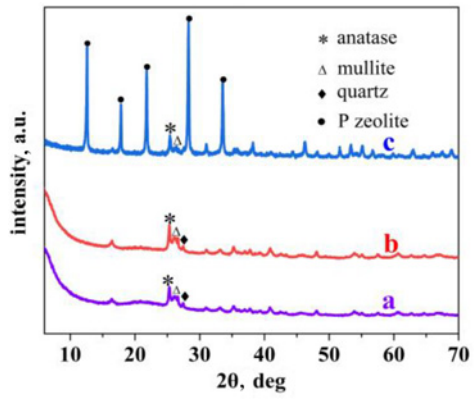


**Fig. 2** *XRD patterns of*
*a* FA
*b* Calcined FA
*c* Zeolite P

with amorphous structure are anatase, quartz and mullite. The diffraction peaks of FA do not change after calcination, indicating that the structure of FA and the crystalline materials in FA do not change under the calcination condition. Fig. 3 illustrates the thermal weight loss-differential thermal curve of FA. As can be seen from Fig. 3, the TG curve of FA is very smooth and there is no obvious weight loss process. At the same time, it can be concluded that the crystalline materials such as mullite, quartz and anatase do not decompose in the temperature range 0–1000°C. It can be concluded from Table 1 that the impurities of FA are mainly organic matters. The organic matters gradually volatilise when the temperature increases, so the weight loss is gradual. However, some strong and sharp diffraction peaks appeared in the synthesised zeolite P sample, indicating the formation of new crystalline minerals. The characteristic reflections for zeolite P appear at $2\theta = 12.605°$, 17.819°, 21.796°, 28.263° and 33.544° which are in compliance with the reference values for a single phase zeolite P according to the Joint Committee on Powder Diffraction Standards (JCPDS) [1, 27]. It can be seen that there is no impurity peak in the sample, which proves that the pure zeolite P structure was obtained successfully. The diffractograms also show the presence of unreacted anatase and mullite, originally present in the FA [18, 26], as shown in Fig. 2*c*. This behaviour is explained by the solubility of these minerals in NaOH and likely reaction medium saturation with Si and Al [26]. The stability of mullite in the hydrothermal synthesis process has also been reported [27]. In addition, the characteristic peak of quartz disappears, indicating that the mineral can be dissolved slowly in the alkaline medium.

Infrared spectroscopy is another important tool for exploring the structure of starting material and final product. The FTIR spectra of FA and calcined FA, as well as synthetic zeolite P at room temperature, was collected to confirm the structure, as shown in Fig. 4.

Figs. 4*b* and *c* show a number of specifically defined FTIR bands in the range of 400–1700 $cm^{-1}$, due to the vibration of Si–O, O–Al, O–Si–O and Al–OH. Owing to internal surface hydroxyl vibration peak and surface hydroxyl stretching vibration peak of FA, the stretching vibration peak of –OH appears in the vicinity of 3445 $cm^{-1}$, as shown in Fig. 4*c*. From Fig. 4*b*, it can be observed that the hydroxyl stretching vibration peak of calcined FA disappears, indicating that the characteristic vibration absorption peak of Al–OH is lost. The reason is the cleavage of the hydroxy bond

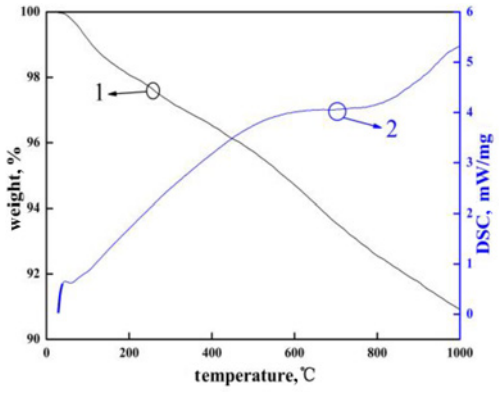


**Fig. 3** *TG–DSC curves of FA (1.TG curve, 2. DSC curve)*

**Table 1** Test results of carbon content of FA (mass fraction/%)

| Moisture (fixed) | Volatile matter | FA | Fixed carbon |
|---|---|---|---|
| 3.31 | 8.76 | 75.69 | 18.52 |

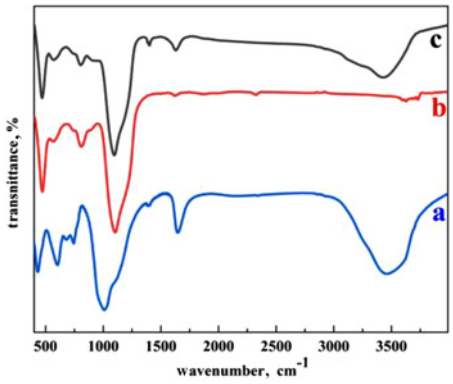


**Fig. 4** *FTIR spectra of*
*a* Zeolite P
*b* Calcined FA
*c* FA

under the action of high temperature. Compared with Fig. 4*a*, the appearance of bands associated with the zeolite structure indicates that the FA is converted to zeolite P. Fig. 4*a* shows strong vibration absorption peaks of the internal tetrahedron at around 1008 and 400–500 $cm^{-1}$. The strongest vibration absorption peak at 1008 $cm^{-1}$ belongs to Si–O or Al–O asymmetric stretching. The vibration absorption peak in the 400–500 $cm^{-1}$ region is ascribed to a Si–O or Al–O bending mode. The absorption peak occurs at ~600–760 $cm^{-1}$ due to the symmetrical stretching vibration of internal tetrahedron [17]. The results show that the zeolite P and [17, 28] matched well, and which confirms once again that pure zeolite P has been synthesised successfully.

Table 2 shows the main chemical compositions of FA and synthetic zeolite P. Since the content of $Fe_2O_3$ is very low, there is no need to do iron removal. Combined with Table 1, the chemical compositions of the unmeasured FA are unburned carbon, fixed moisture as well as some volatile components. Combined with Fig. 4*a*, the synthetic zeolite contains bound water. Compared with FA, the most obvious change is that the content of $TiO_2$ in the synthetic product is increased greatly. The major reason is that the $TiO_2$ gel that is positively charged neutralises the zeolite lattice with a permanent negative charge on the crystallised surface. Other changes are the reduction of silicon content and the slight decrease in aluminium content. The $SiO_2/Al_2O_3$ ratio is reduced from 5.00 to 2.30. The major reason is that the silicon and aluminum, etc. are dissolved in the alkaline solution. At the same time, it is indicated that zeolite P of low $SiO_2/Al_2O_3$ is formed under the synthesis conditions. The soluble silicon dissolved in the alkaline solution continues to react with the aluminium source to synthesise the zeolite P, as shown in Fig 1. In addition, due to the use of 3.0 mol $L^{-1}$ NaOH solution causes the increase of Na content that $Na^+$ is used to balance out the negatively charged zeolite [1].

According to the XRF test, the content of each component in the product is shown in Table 2. According to the molar ratio, the molecular formula of the zeolite P is $6Na_2O{\cdot}10.3SiO_2{\cdot}4.6Al_2O_3{\cdot}12H_2O$. The molecular formula of the synthetic product is basically the same as the ideal molecular formula [2].

3.2. Morphology analysis: Following that, the detailed morphologies of FA and calcined FA as well as synthetic zeolite P were studied by SEM technique, as could be seen in Fig. 5. From Fig. 5*a*, it can be seen that FA of smooth surface is an irregular sheet-like structure under an electron microscope. The edges of the particles are jagged and angular with the particle size of uneven distribution. The major reason is that the inorganic components in the coal are burned at high temperatures and then suddenly cooled in the flue to reduce the surface tension. However, upon calcinations at 800°C for 4 h, the amorphous particles of FA became smaller as compared to Fig. 5*a*. Meanwhile, from Fig. 5*b*, it can

**Table 2** Chemical compositions of raw material and synthesised zeolite (mass fraction/%)

| Compound | $SiO_2$ | $Al_2O_3$ | $Fe_2O_3$ | CaO | $Na_2O$ | $K_2O$ | $TiO_2$ | $P_2O_5$ | MnO | $SiO_2/Al_2O_3$ | Total |
|---|---|---|---|---|---|---|---|---|---|---|---|
| FA | 52.60 | 18.09 | 0.42 | 0.35 | 0.03 | 0.39 | 4.33 | 0.38 | 0.49 | 5.00 | 77.10 |
| synthesised zeolite | 36.63 | 27.50 | 0.87 | 0.55 | 22.02 | 0.29 | 6.01 | 0.03 | 0.01 | 2.30 | 94.20 |

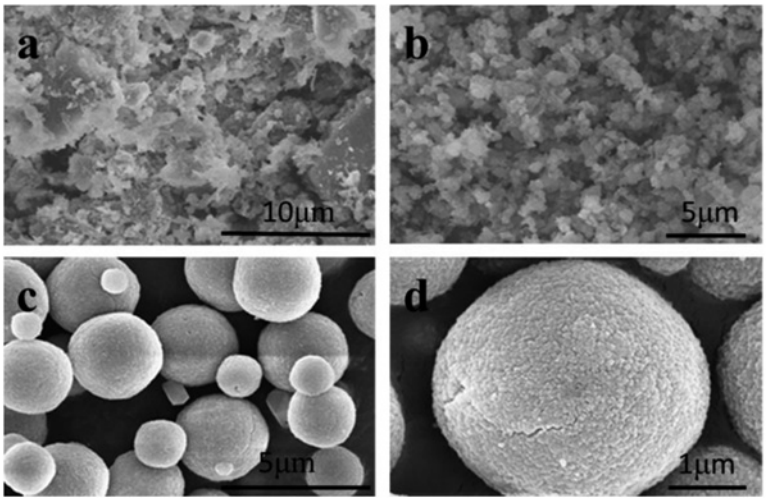


**Fig. 5** *SEM images of*
*a* FA
*b* Calcined FA
c, *d* Zeolite P




doi: 10.1049/mnl.2018.5650

**Table 3** Textural properties of synthesis zeolite P

| Micro pore volume, $cm^3/g$ | Langmuir surface area, $m^2/g$ | BET surface area, $m^2/g$ | Micro pore surface area, $m^2/g$ | External surface area, $m^2/g$ |
|---|---|---|---|---|
| 0.000691 | 49.7412 | 32.2572 | 2.1984 | 30.0588 |

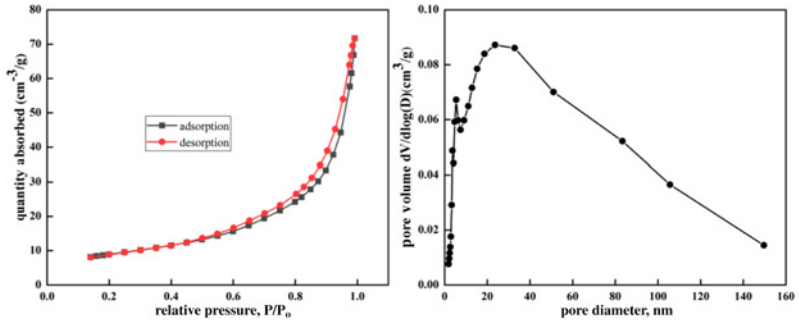


**Fig. 6** *$N_2$ adsorption–desorption isotherms of zeolite P at 77.332 K and pore size distribution of zeolite P*

be observed the appearance of calcined FA with irregular and coarse shape granule. Again, it is shown that the unburned coal and organic matters in the FA can only be removed without changing the crystal form under calcination conditions. Figs. 5*c* and *d* shows the morphology of zeolite P, it can be seen that there is no sheet-like structure in the synthetic zeolite P, and the morphology of the sample evolves from an irregular shape to a spherical shape. Fig. 5*c* shows that each sphere is isolated without aggregation. Fig. 5*d* shows the photomicrograph of zeolite P, which presents pseudo-spherical shape generated from the cluster of acicular crystals, and nanoparticles are distributed on the surface of the sphere. Therefore, the spherical zeolite has a rich pore structure and a large specific surface area, as could be seen in Table 3. As can be seen from Figs. 5*c* and *d*, it is impossible to identify unreacted FA by the SEM images of zeolite P, which is consistent with that observed in the corresponding XRD patterns.

3.3. Analysis of physicochemical properties of zeolite P

3.3.1. BET analysis of zeolite P: The adsorption–desorption isotherm of zeolite P measured with nitrogen gas at 77.332 K, as shown in Fig. 6, shows a typical type IV behaviour. It can be seen that there is the hysteresis loop, which indicates the presence of mesoporosity [29]. It can be seen from Fig. 6 that the adsorption amount in the low-pressure section is gently increased, and the $N_2$ molecules are adsorbed on the inner surface of the mesopores from a single layer to a plurality of layers in this process. Therefore, it is suitable to calculate the specific surface area of the ordered mesoporous material with a relative pressure of 0.10–1.30 by the BET method. The low-pressure isotherm provides information about the microporosity. The micropore surface area and external surface area, as well as micro pore volume, are obtained by the *t*-plot method [30]. The pore size distribution of the micropores has been determined by using the BJH equation as shown in Fig. 6. Textural properties of zeolite P are listed in Table 3. It is because the zeolite P only has eight-membered rings in the structure that all values are rather small compared to normal values in Table 3 [28]. In addition, these values are similar to the reported values in the literature.

3.3.2. Thermal stability analysis: One of the important bases for exploring the properties of zeolite is thermal stability. In our current research, exploring the amount of bound water in synthetic zeolite and the degree of firmness combined with zeolite by thermal analysis of the zeolite. Meanwhile, the phase transition point of the zeolite during heat treatment was studied.

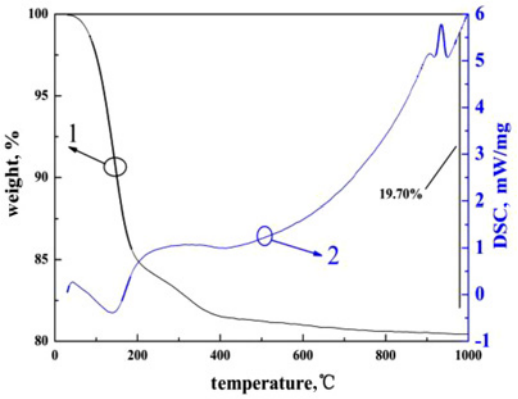


**Fig. 7** *TG–DSC curves of Zeolite P (1. TG curve, 2. DSC curve)*

The TG-DSC curve of the zeolite P is shown in Fig. 7. It can be seen from the TG curve that zeolite P exhibits two mass loss steps. The temperature range of the first event is between 70 and 200°C, with the strongest endothermic peak in the DSC curve at 140°C due to the removal of adsorbed water [31]. When the temperature is up to 200°C, the corresponding weight reduction is about 15.2%. While the second event is in the temperature range of 200–400°C the weight reduction is about 4.5%, which is ascribed to decomposition and removal of the OH group [17]. We can see that the temperature range of the third event is between 400–1000°C, and the endothermic peak in the DSC curve is around 949°C, which is independent of weight losses. This is related to phase transformation, indicating that the crystal structure of the zeolite P has completely collapsed, and creating a new phase. The shape of the TG curve is consistent with the typical behaviour of the synthesised zeolite P [17, 28].

Regarding the thermal behaviour of the synthetic zeolite P, on the one hand, the total water loss of the synthetic zeolite P is 19.7% up to 400°C, which is consistent with the standard zeolite P. This behaviour indicates that it is possible to be a good candidate for detergent builders because they are typically sold in hydrated form wherein the hydrated zeolite weighs about 20–22% water [32, 33]. On the other hand, it has a guiding effect on the heat treatment process of zeolite. The temperature of synthetic zeolite P is controlled below 500°C. It has been reported that the pore structure of the porous material is changed by different heat treatment

temperatures in the literature. The mechanism of how the different calcination temperatures lead to different pore structures is currently being investigated in our laboratory.

**4. Conclusions:** In summary, by carefully adjusting the synthesis conditions, pure zeolite P sample with pseudo-spherical form was successfully synthesised and characterised. The sample was generated from low-grade FA by using the alkali-dissolving hydrothermal method. The XRF study confirmed that the molecular formula of the zeolite P is $6Na_2O{\cdot}10.3SiO_2{\cdot}4.6Al_2O_3{\cdot}12H_2O$. The $N_2$ adsorption–desorption technique indicated the micropore volume, Langmuir surface area, BET surface area, micropore surface area and external surface area of the zeolite P are 0.000691 $cm^3\ g^{-1}$, 49.7412 $m^2\ g^{-1}$, 32.2572 $m^2\ g^{-1}$, 2.1984 $m^2\ g^{-1}$ and 30.0588 $m^2\ g^{-1}$, respectively. The TG-DSC study confirmed that the bound water content of the zeolite P is 19.7% and the phase transition temperature of zeolite P is 400°C. In addition, this simple method of studying thermal stability not only extends the application of zeolite P but can be further extended to other zeolite materials.

**5. Acknowledgments:** This work was supported by the Guizhou Science and Technology Plan Project [(2017) grant no. 7247] and Introducing talent project [Guizhou University, Guiyang (2015) grant no. 13].

## 6 References

[1] Wang F., Wu D.Y., He S.B.: 'Property characterization of NaP1 zeolite from coal fly ash by hydrothermal synthesis', *J. Mater. Eng.*, 2005, **8**, pp. 47–50
[2] Querol X., Moreno N., Umaña J.T., *ET AL.*: 'Synthesis of zeolites from coal fly ash: an overview', *Int. J. Coal Geol.*, 2002, **50**, (1–4), pp. 413–423
[3] Kong D.S., Song S.J., Wang Q.: 'Preparation of P-type molecular sieve from fly ash by alkali melting and hydrothermal method', *Bull. Chin. Ceram. Soc.*, 2016, **35**, pp. 922–926
[4] Murayama N., Yamamoto H., Shibata J.: 'Mechanism of zeolite synthesis from coal fly ash by alkali hydrothermal reaction', *Int. J. Miner. Process.*, 2002, **64**, (1), pp. 1–17
[5] Liu Y., Wang G., Wang L.: 'Zeolite P synthesis based on fly ash and its removal of cu (II) and Ni (II) ions', *Chin. J. Chem. Eng.*, 2018, **128**, pp. 1–8
[6] Masto R.E., Sarkar E., George J.: 'PAHs and potentially toxic elements in the fly ash and bed ash of biomass fired power plants', *Fuel Process. Technol.*, 2015, **132**, pp. 139–152
[7] Lee J., Han S.J., Wee J.H.: 'Synthesis of dry sorbents for carbon dioxide capture using coal fly ash and its performance', *Appl. Energy*, 2016, **131**, pp. 40–47
[8] Luo Y., Ma S., Zhao Z.: 'Preparation and characterization of whisker-reinforced ceramics from coal fly ash', *Ceram. Int.*, 2017, **43**, pp. 1–11
[9] Holler H., Wirsching U.: 'Zeolite formation from fly ash', *Fortschr Miner.*, 1985, **63**, pp. 21–43
[10] Fukasawa T., Horigome A., Tsu T.: 'Utilization of incineration fly ash from biomass power plants for zeolite synthesis from coal fly ash by hydrothermal treatment', *Adv. Powder Technol.*, 2017, **167**, pp. 92–98
[11] Yi L., Chunjie Y., Junjie Z.: 'Synthesis of zeolite P1 from fly ash under solvent-free conditions for ammonium removal from water', *J. Clean. Prod.*, 2018, **202**, pp. 12–22
[12] Jens W.: 'Zeolites and catalysis', *Solid State Ion.*, 1999, **131**, pp. 175–188
[13] Liu X., Wang Y., Cui X., *ET AL.*: 'Influence of synthesis parameters on NaA zeolite crystals', *Powder Technol.*, 2013, **243**, pp. 184–193
[14] Dufour J., Gonzalez V., La Iglesia A.: 'Optimization of 4A zeolite synthesis as recovery of wastes from aluminum finishing', *J. Environ. Sci. Health A*, 2001, **36**, pp. 1257–1269
[15] Xu R., Pang W.Q.: 'Molecular sieve and porous mateials chemisty' (Science Press, Bejing, 2004)
[16] Xu R., Pang W. Q., Tu K. G.: 'Zeolite molecular sieves structure and synthesis' (Jilin University Press, Changchun, 1987)
[17] Huo Z., Xu X., Zhi L.: 'Synthesis of zeolite NaP with controllable morphologies', *Micropor. Mesopor. Mater.*, 2012, **158**, pp. 137–140
[18] Cardoso A.M., Paprocki A., Ferret L.S.: 'Synthesis of zeolite Na-P1 under mild conditions using Brazilian coal fly ash and its application in wastewater treatment', *Fuel*, 2015, **139**, pp. 59–67
[19] Bessa R.D.A., Costa L.D.S., Oliveira C.P.: 'Kaolin-based magnetic zeolites A and P as water softeners', *Micropor. Mesopor. Mater.*, 2017, **245**, pp. 64–72
[20] Albert B.R., Cheetham A.K., Stuart J.A.: 'Investigations on P zeolites: synthesis, characterisation, and structure of highly crystalline low-silica NaP', *Micropor. Mesopor. Mater.*, 1998, **21**, pp. 133–142
[21] Cao J.L., Liu X.W., Fu R.: 'Magnetic P zeolites: synthesis, characterization and the behavior in potassium extraction from seawater', *Sep. Purif. Technol.*, 2008, **63**, pp. 92–100
[22] Huang Y., Dong D., Yao J.: 'In situ crystallization of macroporous monoliths with hollow NaP zeolite structure', *Chem. Mater.*, 2010, **22**, pp. 5271–5278
[23] Silva F.A.D., Rodrigues A.E.: 'Propylene/propane separation by vacuum swing adsorption using 13X zeolite', *AiChE. J.*, 2010, **47**, pp. 341–357
[24] Habibi D., Nasrollahzadeh M., Sahebekhtiari H.: 'Green synthesis of formamides using the natrolite zeolite as a natural, efficient and recyclable catalyst', *J. Mol. Catal. A-Chem.*, 2013, **378**, pp. 148–155
[25] Kong D., Li L., Fan J.X., *ET AL.*: 'Preparation of P type molecular sieves from gangue of high iron and high silica content', *Bull. Chin. Ceram. Soc.*, 2013, **32**, pp. 1052–1056
[26] Cardoso A.M., Horn M.B., Ferret L.S.: 'Integrated synthesis of zeolites 4A and Na–P1 using coal fly ash for application in the formulation of detergents and swine wastewater treatment', *J. Hazard Mater.*, 2015, **287**, pp. 69–77
[27] Berkgaut V., Singer A.: 'High capacity cation exchanger by hydrothermal zeolitization of coal fly ash', *Appl. Clay Sci.*, 1996, **10**, pp. 369–378
[28] Breck D.W., 'Zeolite Molecular Sieves: Structure, Chemistry and Use' (John Wiley and Sons, New York, USA, 1974), pp. 499
[29] Gholipour F., Mofarahi M.: 'Adsorption equilibrium of methane and carbon dioxide on zeolite 13X: experimental and thermodynamic modeling', *J. Supercritit Fluid*, 2016, **111**, pp. 47–54
[30] Garshasbi V., Jahangiri M., Anbia M.: 'Equilibrium $CO_2$, adsorption on zeolite 13X prepared from natural clays', *Appl. Surf. Sci.*, 2016, **393**, pp. 225–233
[31] Pal P., Das J. K., Das N.: 'Synthesis of NaP zeolite at room temperature and short crystallization time by sonochemical method', *Ultrason. Sonochem.*, 2013, **20**, (1), pp. 314–321
[32] Ayele L., Pérez-Pariente J., Chebude Y.: 'Synthesis of zeolite A from Ethiopian kaolin', *Micropor. Mesopor. Mater.*, 2015, **215**, pp. 29–36
[33] Georgiev D., Bogdanov B., Markovska I.: 'A study on the synthesis and structure of zeolite NaX', *J. Univ. Chem. Technol. Metall.*, 2013, **48**, pp. 168–173




doi: 10.1049/mnl.2018.5650